JTTEE5 10:487-496

Peer Reviewed

Effect of the Increase in the Entrance Convergent Section Length of the Gun Nozzle on the High-Velocity Oxygen Fuel and Cold Spray Process

K. Sakaki and Y. Shimizu

(Submitted 24 October 2000)

Nozzle geometry, which influences combustion gas dynamics and, therefore, sprayed particle behavior, is one of the most important parameters in the high-velocity oxygen-fuel (HVOF) thermal spray process. The nozzle geometry is also important in the cold spray method. The gas flows in the entrance convergent section of the nozzle exhibit a relatively higher temperature and are subsonic; thus, this region is most suitable for heating spray particles.

In this study, numerical simulation and experiments investigated the effect of the entrance geometry of the gun nozzle on the HVOF process. The process changes inside the nozzle, as obtained by numerical simulation studies, were related to the coating properties. An Al_2O_3-40 mass% TiO_2 powder was used for the experimental studies. The change in entrance convergent section length (rather than barrel part length or total length) of the gun nozzle had a significant effect on the deposition efficiency, microstructure, and hardness. The deposition efficiency and hardness increased as this geometry increased. On the other hand, the calculated and measured particle velocity showed a slight decrease. This effect on the HVOF process will also be applied to the nozzle design for the cold spray method.

Keywords Al_2O_3-40 mass% TiO_2, cold spray, HVOF, nozzle design, numerical simulation

1. Introduction

High-velocity oxygen-fuel (HVOF) thermal spray systems and spray materials for them have been developed over the last decade. As a result, the fields of application of the HVOF thermal spraying are expanding rapidly.

One of the major characteristics of the HVOF process is the high-speed gas jet, which is governed by gas dynamics. In gas dynamics, supersonic flows are obtained with convergent-divergent nozzle, which are used for rocket motors. Rocket motors, including their nozzle design, have been studied and analyzed in detail. While the principal purpose of the design of a rocket motor nozzle is to maximize the thrust, in thermal spraying, the main purpose is to obtain better coating quality.

The HVOF systems employ various kinds of gun nozzle contours, such as convergent-barrel,[1,2] convergent-divergent (or de Laval nozzle),[3] convergent-multistage divergent,[4] and convergent-divergent-barrel.[5,6] The HVOF gun systems without any nozzle are also in use.[3]

Previous studies on thermal spraying show that the coating properties are principally determined by the thermal and kinetic energy states of particles upon impact with the substrate. In order to have a balance between these two states; various changes in the design of the HVOF gun nozzle have been attempted. However, the works concerning the influence of nozzle geometry on the thermal spray process are sparse.[7,8,9]

Previously, we have considered the effect of throat diameter and exit divergence of the gun nozzle on the HVOF process.[8,10,11] The combustion gas flow (such as pressure, velocity, temperature, and expansion state of gas jet from the nozzle exit), the particle behavior, and, therefore, the nature of coatings were found to be significantly influenced by these nozzle parameters. In addition, the effect of the expansion state of the combustion gas jet on the HVOF process was investigated using a diverging nozzle exit. The particle velocity reached a maximum with the correct expansion state of the gas jet due to an increased gas jet velocity. This resulted in an increase in the bonding strength of the NiCrAlY coating.[12]

In the present study, the effect of increasing the length of the entrance convergent section of the nozzle on the HVOF thermal spraying process is investigated by a numerical simulation and experiments with a Jet Kote™ system (Stellite Coatings, Goshen, IN). The gas flow in the entrance convergent section of the nozzle is of relatively higher temperature and is subsonic; therefore, this region will be convenient for heating of the high-melting-point spray materials such as ceramics and refractory metals. The goal of this investigation is to establish a design for the HVOF gun nozzle in order to gain better coating quality of any material powder.

The nozzle geometry is also important with regard to the cold spray method.[13] In the cold spray method, a coating is formed by exposing a substrate to high velocity solid-phase particles, which have been accelerated by supersonic gas flow at a tem-

K. Sakaki and **Y. Shimizu,** Faculty of Engineering, Shinshu University, Watasato 4-17-1, Nagano 380-8553, Japan. Contact e-mail: ksakaki@gipwc.shinshu-u.ac.jp.

Peer Reviewed

Nomenclature	
C_d	drag coefficient
c_p	specific heat of particle, J/(kg K)
D_p	particle diameter, m
d	nozzle diameter, m
h	heat transfer coefficient, kW/(m^2 K)
L	latent heat of fusion of particle material, kJ/kg
l	nozzle total length, m
l_{conv}	nozzle convergent part length, m
l_{div}	nozzle divergent part length, m
P	gas pressure, Pa
Q	heat from gas to particle, J
Q_f	heat of fusion of particle, J
U	velocity, m/s
U_{pcr}	critical velocity, m/s
T	temperature, K
T_f	film temperature, K
T_{mp}	melting point of particle, K
t	time, s
ψ	nozzle intake angle, deg
κ	specific heat ratio of gas
ρ	density, kg/m^3
Subscripts	
g	gas
p	particle
i	nozzle intake
t	nozzle throat
e	nozzle exit
s	nozzle straight part

perature much lower than the melting or softening temperature of the feedstock. The effect in the HVOF process will also be applied to the nozzle design for the cold spray method. The influence of nozzle geometry and gas initial conditions on the cold spray process (*i.e.*, the behavior of the carrier gas and spray particles) within the nozzle is investigated by a numerical simulation prior to designing the cold spray equipment and producing coatings.

2. Experimental Equipment and Methods

2.1 HVOF Thermal Spray Equipment

The Jet Kote™ HVOF thermal spray system with a mass flow controller attachment was used for the present study. A schematic diagram of the Jet Kote™ gun and nozzle are shown in Fig. 1. Propylene, C_3H_6, gas was used as the fuel and the spray conditions used are given in Table 1. Some technical characteristics of this system are that it (1) employs an internal combustion chamber to generate the hot, extreme velocity exhaust jet to spray, and (2) injects powder axially into the center of the exhaust gas jet at the nozzle intake. In this system, combustion gas flows from the combustion chamber through four holes in the combustion head (changing its direction at a right angle) to the nozzle intake with an initial velocity of U_{gi}.

In order to study effects of the gun nozzle geometry, on the combustion gas behavior, spray particles, and coating properties, two different nozzle shapes, namely, a "straight nozzle" (equal to factory standard-made barrel one) and a "convergent nozzle," were used for the present study. Further, the dimensions such as total length l of the straight nozzle and convergent length l_{conv} at the entrance of the convergent nozzle were varied, as shown in Table 2. The length l of a straight nozzle (in the following, straight nozzle is indicated by "total nozzle length $l - S$") was varied to three different levels: 76.5 mm (3 in.), 156.2 mm (6 in.), and 304.8 mm (12 in.). A convergent nozzle (in the following, the converging nozzle is indicated by "l—length of entrance convergent part l_{conv} Conv") was made by increasing the l_{conv} of the straight nozzle shown in Fig. 1. The throat diameter d_t and exit diameter d_e were fixed at 7.8 mm.

2.2 Thermal Spray Powder

NiCrAlY alloy powder of Ni-13Cr-5Al-0.5 mass% Y composition (Shocoat^R MA-90, gas atomized powder (Showa Denko, Tokyo)) was used for the present study. An increase in the entrance part of the nozzle can cause an increase in the heat input of particles and oxidize NiCrAlY particles. Therefore, Al_2O_3-40 mass% TiO_2 powder (Shocoat^R K-40F, crashed powder) was also used. Properties of these powders are shown in Table 3.

2.3 Evaluation Approach

The expansion states of HVOF jets from the gun nozzle exit with nozzles used without spray powder were evaluated by means of visual observation and by photographic methods. The nozzle intake pressure was measured through a powder feed port by a pressure indicator (PF-30KF, Kyowa Electronic Instrument, Tokyo).[10] The velocity surface temperature and diameter of the sprayed particles during HVOF spraying were measured using an in-flight particle measurement system, namely, the DPV-2000 (Tecnar Automation Ltd., St-Bruno, QC, Canada), which detects the thermal radiation emitted by hot in-flight particles.[14]

The nature of sprayed coatings was characterized by means of electron probe microanalysis (EPMA), microhardness, and X-ray diffraction analysis.

The deposition efficiency was ascertained by measuring the weight gain on mild steel substrates of 75 × 105 × 6 mm dimensions for a spray time of 30 s taking into account the known feedstock powder flow rate.

3. Numerical Simulation of Thermal Spray Process

3.1 HVOF Process

There are several techniques that can be used to calculate the gas flow of HVOF systems. Recent analyses have used computational fluid dynamics (CFD) methods to simulate this complex phenomenon in two dimensions. In the present paper, the internal nozzle flow was treated as quasi-one-dimensional isentropic flow. This one-dimensional approximation is simple and sufficiently correct for the present purpose of expressing an effect of

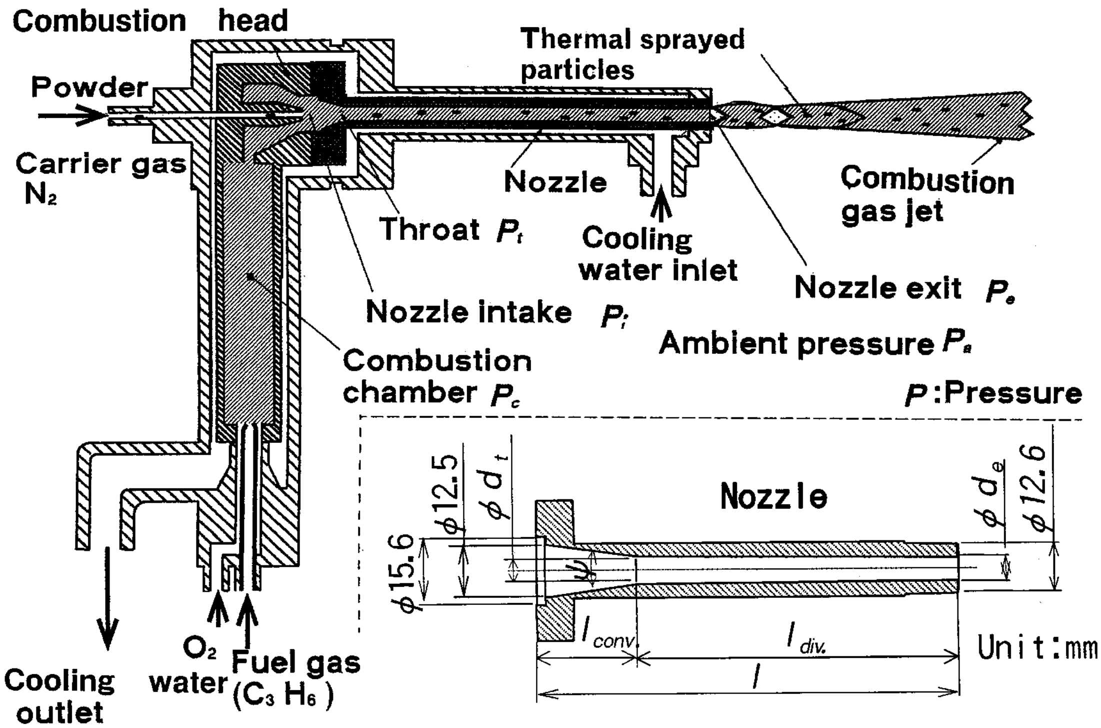

Fig. 1 Schematic diagram of HVOF (Jet Kote™) spraying gun and nozzle

Table 1 HVOF spraying parameters and initial condition

Fuel/oxygen flow rate (C_3H_6/O_2): 90/486 L/min (normal)
Carrier gas (N): 35 L/min (normal)
Powder feed rate: 7.7 cm^3/min
(NiCrAlY alloy: 55 g/min, and Al_2O_3-40 mass% TiO_2: 12 g/min)
Gun traverse speed: 100 mm/s, gun traverse pitch: 5 mm
Spray distance: 200 mm
Substrate: SUS304, SS400
⟨Initial conditions for numerical simulation⟩
Particle velocity U_{pi}: 10 m/s
Particle temperature T_{pi}: 300 K

nozzle geometry on the internal nozzle flow.[10] Detailed derivation of the modeling can be found in Ref 10 and 11. A brief description of the simulation is given below.

Modeling of Combustion Gas Flow within the Nozzle. The following assumptions were made to model the gas flow in the HVOF gun nozzle.[10]

- Combustion gas flow within the nozzle is the quasi-one-dimensional isentropic flow of semiperfect gas.
- The chemical reaction of combustion in the combustion chamber follows as Eq 1 so that combustion gas is composed only of CO_2, H_2O (gas), excessive O_2, and carrier gas N_2.

$$C_3H_6 + (9/2 + X)O_2 + YN_2 = 3CO_2 + 3H_2O + XO_2 + YN_2 + 1926[\text{kJ/mol}] \quad \text{(Eq 1)}$$

- Combustion gas flows from the combustion chamber to the nozzle intake with an initial velocity U_{gi}, temperature T_{gi}, and pressure P_i.
- Principles of heat transfer only apply to heat exchange between the hot combustion gas and combustion chamber wall/cooling water.

In this manner, the pressure P, density ρ_g, temperature T_g, and velocity U_g of the gas flow can be calculated from the ratio of the nozzle cross-sectional area at a given point to the nozzle throat area.[15]

Modeling of Particle Behavior within the Nozzle. Particle acceleration and heating in a gas flow within the nozzle are given by solving the equations of motion and heat transfer, as described below. These equations in the present paper are based on the following four assumptions.

- The spray particle is spherical with negligible internal temperature gradients.
- The particle specific heat is independent of its temperature and constant.
- The gravitational effect and the interaction between particles are ignored.
- The influence of particles on gas flow are neglected. This is equivalent to stating that the gas energy decrease along the nozzle due to acceleration and heating of the particle is neglected.

Under the above assumptions, the equations of motion of a particle in the HVOF process can be written as

$$\frac{dU_p}{dt} = \frac{3}{4}\frac{C_d}{D_p}\frac{\rho_g}{\rho_p}\left(U_g - U_p\right)\left|U_g - U_p\right| \quad \text{(Eq 2)}$$

where U_p is the particle velocity, t is time, C_d is the drag coeffi-

Table 2 Shape and size of gun nozzle used and state of combustion gas stream

Nozzle	d_t(mm)	ψ_o(°)	d_e(mm)	l {in}(mm)	l_i(mm)	l_s(mm)	P_i(a) MPa (abs)	P_e(b) MPa (abs)	U_{ge}(b) m/s	T_{ge}(b) K	Gas jet(c)
12S7.8(d)		(60)		304.8{12}	8.9	295.9	0.42	0.245	1055	2832	Weak underexpansion
6S7.8(d)		(60)		156.2{6}	8.9	143.7	0.42	0.245	1055	2832	Weak underexpansion
3S7.8(d)	7.8	(60)	7.8	76.2{3}	8.9	67.3	0.42	0.245	1055	2832	Underexpansion
3-26Conv.7.8		12		76.2{3}	25.5	50.7	0.42	0.245	1055	2832	Underexpansion
3-48Conv.7.8		6		76.2{3}	48.0	28.2	0.42	0.245	1055	2832	Underexpansion

(a) Measured mean value, (b) calculated value, (c) results of observation of HVOF free jet by photography, and (d) on the market
Nomenclature: d—nozzle diameter, ψ—nozzle intake angle, l—nozzle length, P—pressure, U—velocity, and T—temperature
Subscripts: g—combustion gas, i—nozzle intake, t—nozzle throat, e—nozzle exit, and s—nozzle straight part

Table 3 HVOF spraying powder properties

Property	NiCrAlY	Al_2O_3-40 mass% TiO_2
Diameter, μm	10 to 45(30)(a)	5 to 25(12)(a)
Melting point, K	1727	2133
Density, kg/m^3	8300	3710
Specific heat, J/(kg K)	444	1183
Latent heat of fusion $\times 10^6$ J/kg	0.3	1.0

(a) Mean diameter of powder

cient, D_p is the particle diameter, ρ_g is the combustion gas density, ρ_p is the particle density, and U_g is the gas velocity. The term C_d for sphere is a function of the particle Reynolds number.[16]

Heating of a particle in a gas flow can be expressed as follows:

$$\frac{dT_p}{dt} = \left(T_g - T_p\right)\frac{6h}{c_p \rho_p D_p} \quad \text{(Eq 3)}$$

where T_p is the particle temperature, T_g is gas temperature, h is the heat-transfer coefficient, and c_p is the specific heat of the particle. The heat-transfer coefficient h in Eq 3 can be found by means of the semiempirical Ranz-Marshall equation, in which h is a function of the Reynolds number and the Prandtl number. The influence of radiant heat between the combustion gas and particle was neglect.

For the calculation of the Reynolds number and the Prandtl number, the values of the specific heat of gas, the gas viscosity, and the gas thermal conductivity are used in the film temperature T_f, which is defined by[17]

$$T_f = (T_g + T_p)/2 \quad \text{(Eq 4)}$$

When T_p reaches the melting point of the particle T_{mp}, the heat from the gas to particle, Q, will be the heat of fusion of the particle. The particle state is represented by the degree of melting of the particle as follows:

$$\frac{\sum Q}{Q_f} = \frac{h\int\left(T_g - T_{mp}\right)dt}{\rho_p D_p L} \quad \text{(Eq 5)}$$

where Q_f is the heat of fusion per particle and L is the latent heat of fusion of the particle material.

Numerical Approximation of the HVOF Process. An outline of a numerical approximation of the HVOF process is as follows: (1) initial conditions were given; (2) the pressure P, the temperature T_g, and the velocity U_g of the gas flow were calculated from the ratio of the cross-sectional area of the nozzle at the intake point to the nozzle throat area; (3) the above differential equations (Eq 2 and 3) concerning particle behavior were solved numerically by the Euler method; and (4) the processes of (2) and (3) were repeated from the nozzle intake to the nozzle exit.

The thermal spray condition data and the initial conditions shown in Table 1 (except the powder feed rate and the spray distance) were used. The values of diameter, density, melting point, specific heat, and latent heat of fusion of the spray powder used in calculation are given in Table 3.

3.2 Cold Spray Process

The results provided by this simulation could be a little larger than the real values because of the above assumptions.

A conceptional drawing of the cold spray equipment for the present study is shown in Fig. 2. Compressed nitrogen gas is introduced to a heater and a powder feeder. The pressure gas is heated in an electric furnace. Feedstock powder is injected axially and centrally into the gas flow at the gun nozzle intake. The spray gun is fitted with a convergent-divergent nozzle (or a conical de Laval nozzle) designed to produce a correct expansion gas jet,[8] which is supersonic at its exit, and free shock diamonds. Namely, the nozzle exit pressure P_e of the gas fed at varied nozzle intake pressures P_i matches the ambient pressure by changing the exit diameter d_e. The total nozzle length l and throat diameter d_t are fixed at 300 and 5 mm, respectively.

Spray powder used in this study is Ni-Al bronze, since prior studies[13] have created a coating with this powder by the cold spray method. Alkimov *et al.* have reported that there exists a critical velocity U_{pcr} for each coating and substrate material combination, above which the particles have sufficient kinetic energy to build a coating.[18] The value of U_{pcr} for a Ni-Al bronze particle in the present study is 600 m/s, because typical values of U_{pc} for copper, zinc, nickel, and iron range from 550 to 650 m/s for a copper substrate.[18]

The spray parameters used in this simulation are shown in Table 4. The basic treatment for the cold spray simulation is the same as that for HVOF simulation. The same assumptions as applied to the HVOF process were made to model the cold

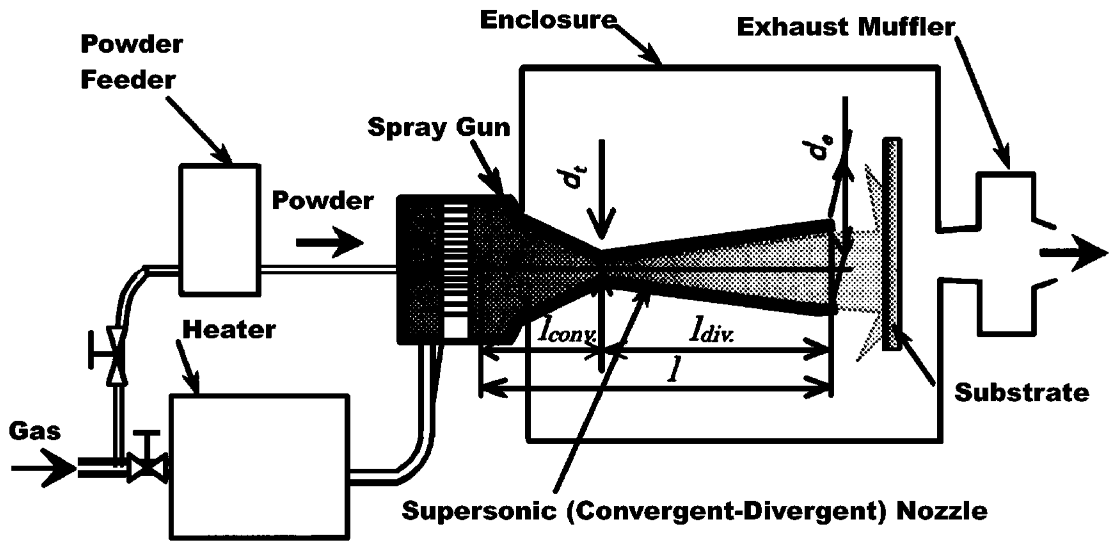

Fig. 2 Conceptual drawing of the cold spray equipment

Table 4 Initial conditions of cold spray process simulation

Gas: N_2
Gas initial pressure P_i: 0.5–5.0 (2.0) MPa (abs)
Gas initial velocity U_{gi}: 0–100 (0) m/s
Gas initial temperature T_{gi}: 300–2000 (750) K
Powder: Ni-Al bronze
(melting point: 1340 K, density: 7600 kg/m^3, specific heat: 440 J/(kg K), latent heat of fusion: 0.205 × 10^6 J/kg
Diameter: 1–50 (20) μm
Particle velocity U_{pi}: 0–100 (10) m/s
Particle temperature T_{pi}: 300 K
The baseline condition is shown in parentheses

spray process with an additional one that the gas flow within the nozzle is the quasi-one-dimensional isentropic flow of semiperfect gas.

The equations of motion and heating of a particle in the cold spray process can be written as Eq 2 and 3 under the above assumptions. An important distinction between the modeling of the two processes is that the influence of radiant heat of the gas on the particle might be neglected, since the gas temperature is lower. The numerical approximations of the cold spray process and of the HVOF process are basically the same.

4. Results and Discussion

4.1 Effect of Increasing the Nozzle Entrance Convergent Section Length on the HVOF Thermal Spraying Process

The numerical simulation results on the effect of increasing the nozzle entrance convergent section length l_{conv} on gas velocity U_g, temperature T_g, particle velocity U_p, and other properties are given in Fig. 3 and as part of Table 2. The results show that the gas flow in the entrance convergent section of the nozzle is of a higher relative temperature and is subsonic. Therefore, the degree of particle melting Q/Q_L increases and U_p decreases slightly with increasing l_{conv}. The calculated U_{pe} agreed approximately with the values measured by the in-flight particle measurement system for NiCrAlY HVOF processes in change with l_{conv}. This tendency was confirmed by observing the nature of the sprayed coatings; namely, cross-sectional hardness and oxygen content of NiCrAlY coatings increase and deposition efficiency decreases with increasing l_{conv}. As an example of the effect of an increase in l_{conv} on the coating property, surface structures of Al_2O_3-40 mass% TiO_2 coatings are shown in Fig. 4, in which coatings sprayed with a longer nozzle by HVOF and by plasma spray are compared.

It was found that splat morphologies vary with l_{conv} and nozzle length l, because input heats of particles from the gas or degree of melting increase with increasing l_{conv} and l.

Figure 5 shows some typical structures of Al_2O_3-40 mass% TiO_2 splats sprayed by HVOF and collected on 304 stainless steel substrates at room temperature. In order to obtain isolated splats, a shielding plate on which several holes of 1 mm were distributed was placed parallel to the substrate at a distance of about 5 mm. The splat patterns are roughly divided into the following three categories: (a) unmolten particles, (b) semimolten particles, and (c) molten particles with splash. The different morphologies arise due to variations in the input heat of particles, substrate temperature, and impact velocity of particle to substrate. From (a) to (c), the input heat of particles increases.

The proportion of the various splat patterns of Al_2O_3-40 mass% TiO_2 powder with respect to a change in the nozzle entrance convergent section length l_{conv} is shown in Fig. 6. In this figure, the percentage of splat morphology (b) semimolten particles and (c) molten particles with splash increases slightly with l_{conv} at three 76.2 mm (3 in.) nozzles (from 3S, 3-26Conv to 3-48Conv nozzle). This tendency shows that an increase in l_{conv} causes an increase in the gas input heat of particles.

Figure 7 shows the results of the deposition efficiency, the calculated degree of melting of particles, and the cross-sectional hardness of Al_2O_3-40 mass% TiO_2 coatings with respect to a

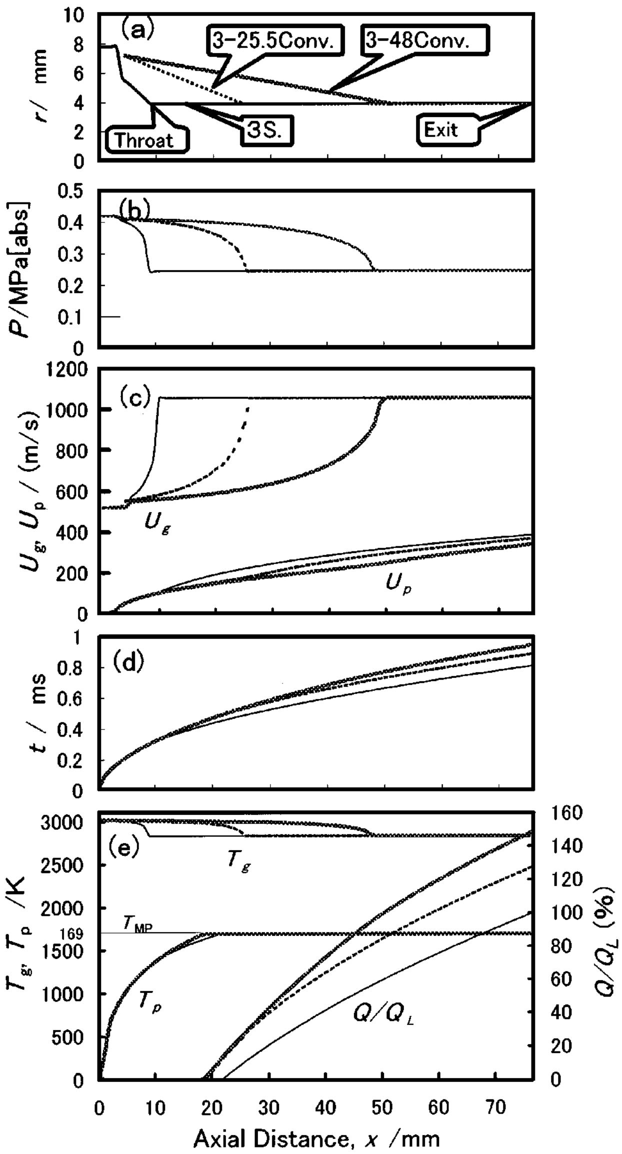

Fig. 3 Effect of the increase in nozzle entrance convergent section length (for three nozzle shapes) on the calculated results of the (**a**) nozzle contour, (**b**) gas pressure, (**c**) velocity of gas and particle, (**d**) particle resident time, and (**e**) temperature of gas and particles and the degree of melting particle

change in l_{conv} and total nozzle length l. The figure shows an increase in deposition efficiency and coating hardness with an increase in l_{conv}. Moreover, the deposition efficiency and the cross-sectional hardness of the coating with 3-48Conv nozzle are higher than those with longer nozzles such as 12S and 6S. This result can be explained from heat losses by nozzle cooling and pipe fraction loss, which were observed in terms of the expansion state of the gas jet shown in Table 2. Therefore, these losses increase with the nozzle length, so that velocity and temperature of the gas and particles decrease with an increase in the nozzle length.

In summary, the effect of increasing the entrance convergent section length of the nozzle on the heating particle is larger than that of increasing the barrel part length or total nozzle length in the HVOF thermal spraying process. Therefore, a combination of increasing the entrance convergent section length and the total length of the nozzle is more effective.

4.2 Influence of Gas Initial Conditions and Nozzle Geometry on the Cold Spray Process

The influence of gas initial conditions and nozzle geometry on the cold spray process (behavior of carrier gas and spray particles) within the nozzle is investigated by a numerical simulation.

Influence of Particle Diameter. The numerical simulation results (gas velocity U_g, temperature T_g, particle velocity U_p, and temperature T_p) with a change in the particle diameter of Ni-Al-bronze powder are given in Fig. 8. The entrance convergent length l_{conv} of the conical de Laval nozzle used is 9 mm, and the following initial conditions are used as baseline conditions: gas pressure of 2.0 MPa (abs), temperature T_{gi} of 750 K, velocity U_{gi} of 0 m/s, particle temperature T_{pi} of 300 K, and velocity U_{pi} of 10 m/s.

Using the conical de Laval (convergent-longer divergent) nozzle, the gas velocity U_g increases along the axial distance within the nozzle to reach 950 m/s (Mach number M of 2.7) at the nozzle exit, and the gas temperature decreases to reach 290 K (which is equal to room temperature).

Figure 8 shows that the particles, even the larger ones, are accelerated and heated very quickly. The results indicated that 20 m and smaller particles reach the critical velocity of 600 m/s before arriving at the nozzle exit and attain the gas temperature within the entrance convergent part of the nozzle.

The value of T_g becomes lower than T_p in the nozzle, because the heat capacity of the gas is much lower than that of the particle and the gas initial temperature is much lower. In conventional thermal spray processes such as HVOF, plasma spray, and so on, using higher-temperature gas, this tendency is not observed.

Influence of Gas Initial Conditions. Figure 9 shows the effect of initial gas pressure P_i on the cold spray process (velocity of gas U_{ge} and particle U_{pe}, temperature of gas T_{ge}, and particle T_{pe} at nozzle exit) with nozzles designed to produce perfectly the expansion gas jet according to P_i. In the figure, U_{ge} and U_{pe} increase with an increase in P_i. Particles 20 μm and smaller reach the critical velocity U_{pcr} at P_i above 2 MPa. However, 50 μm and larger particles cannot attain this velocity at P_i up to 5 MPa. The values of T_{ge} and T_{pe} decrease with increasing P_i. For example, T_{ge} at P_i of 5 MPa drops to 200 K (or −73 °C).

The effect of gas initial temperature T_{gi} on the cold spray process under the baseline conditions, except for T_{gi}, is provided (Fig. 10). At most, the gas for cold spray might be used at a temperature up to 1000 K. In this figure, the results up to 2500 K are shown in order to compare them with the results of the HVOF process. The values of U_{ge} and U_{pe} increase with T_{gi}. The value of U_{pe} is higher than that of U_{pcr} at T_{gi} above 700 K. It is clear that the minimum T_{gi} exists for these initial gas pressures, which allows particles to reach U_{pcr}. For the HVOF process, the pressure of the combustion gas is lower than that of the cold spray gas because the temperature of the combustion gas is much higher.

The effect of the initial gas velocity, U_{gi}, on the cold spray process under the baseline conditions except, for U_{gi}, is indicated in Fig. 11. With an increase in U_{gi}, U_{ge} and U_{pe} increase slightly,

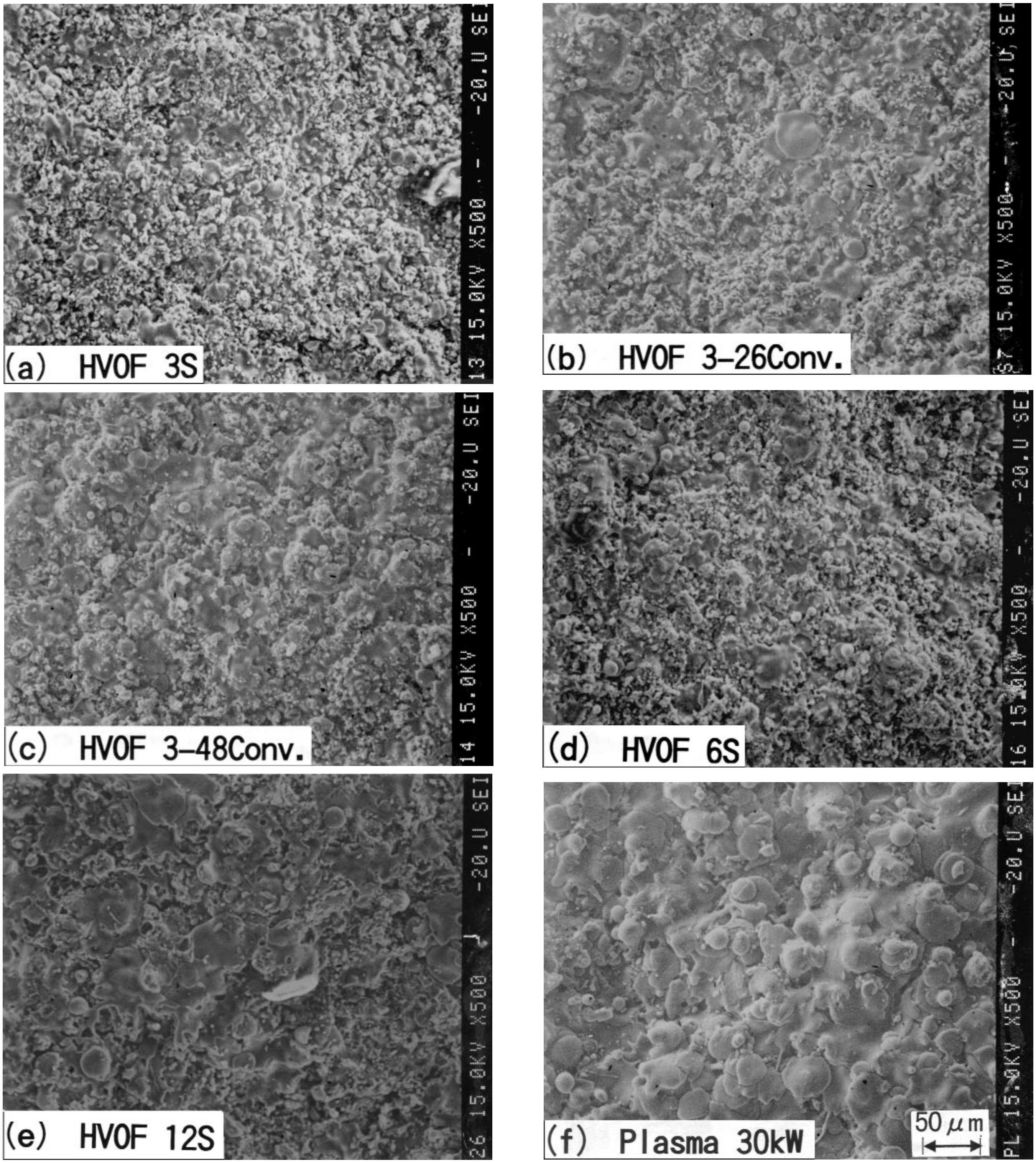

Fig. 4 Surface SEM structures of Al_2O_3-40 mass% TiO_2 coatings sprayed by HVOF (with several nozzle shapes) and plasma spraying. 3S is a 3 in. straight nozzle, 3-26Conv is a 3 in. converging nozzle with a 26 mm converging part length, 3-48Conv is a 3 in. converging nozzle with a 48 mm converging part length, 6S is a 6 in. straight nozzle, and 12S is a 12 in. straight nozzle

while T_{ge} and T_{pe} decrease slightly. To heat powder effectively, gas might be supplied to the nozzle at a lower velocity. However, particle behavior is independent of the gas initial velocity up to 100 m/s.

Influence of Increases in the Nozzle Entrance Convergent Section Length. The effect of increases in the nozzle entrance convergent section length, l_{conv}, on the cold spray process under the baseline conditions is given in Fig. 12. The value of T_{pe} in-

Fig. 5 Typical patterns of the structure of Al_2O_3-40 mass% TiO_2 splats sprayed by HVOF collected on 304 stainless steel substrate: (**a**) unmolten particle with trusting, (**b**) semimolten particle, and (**c**) molten particle with splash

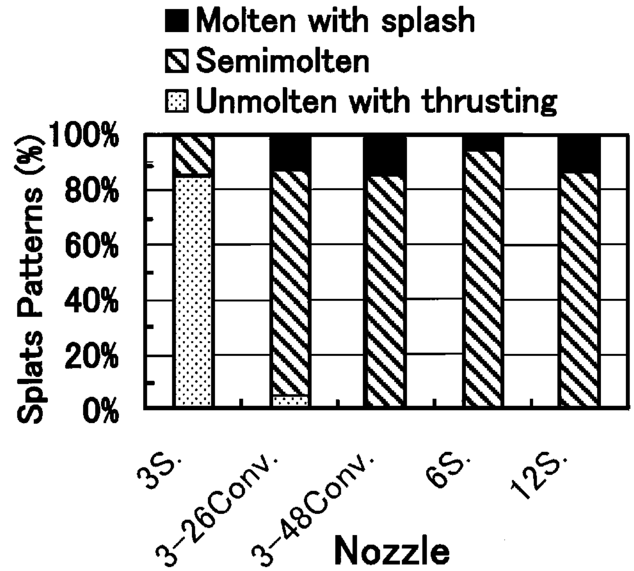

Fig. 6 Percentage of patterns of the structure of Al_2O_3-40 mass% TiO_2 splats sprayed by HVOF with a change in nozzle shape. 3S is a 3 in. straight nozzle, 3-26Conv is a 3 in converging nozzle with 26 mm converging part length, 3-48Conv is a 3 in converging nozzle with 48 mm converging part length, 6S is a 6 in. straight nozzle, and 12S is a 12 in straight nozzle

crease steadily and T_{ge} increases slightly, while U_{pe} decreases steadily and U_{ge} decreases slightly with increasing l_{conv}. Therefore, increasing l_{conv} effects particle heating but does not accelerate it in the same fashion as for HVOF. Thus, l_{conv} must be up to 100 mm under these spray conditions to obtain a critical velocity of 600 m/s. However, now the influence of particle and substrate temperatures on the critical velocity is not revealed. Increasing l_{conv} in order to lower the critical velocity can raise the particle temperature.

5. Conclusions

Numerical simulation and experiments have investigated the effect of increasing the nozzle entrance converging section on the HVOF process. The numerical simulations also investigate this effect with regard to the spray parameters of the cold spray process. The results are summarized as follows.

- The particle temperature or the degree of melting of particles increases, but the particle velocity decreases slightly with an increase in the entrance convergent section length of the nozzle of HVOF and cold spray equipment. Therefore, increasing this length has an effect on particle heating.
- The surface structure and morphology of the splat pattern of Al_2O_3-40 mass.% TiO_2 coatings sprayed by HVOF vary with an increase in the nozzle entrance convergent section length.
- Deposition efficiency and cross-sectional hardness of Al_2O_3-40 mass% TiO_2 coatings sprayed by HVOF significantly increase with the nozzle entrance convergent section length.
- In cold spray, gas velocity increases along the axial distance within the nozzle to reach 950 m/s (Mach number of 2.7) at

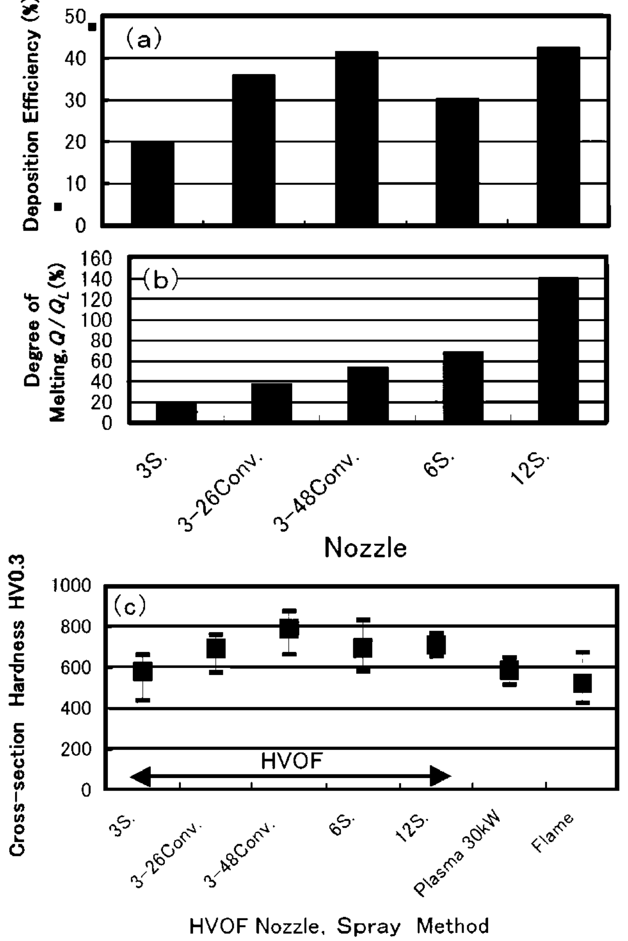

Fig. 7 Effect of nozzle shape on (**a**) deposition efficiency, (**b**) degree of melting of particle, and (**c**) cross-sectional hardness of sprayed Al_2O_3-40 mass% TiO_2 coatings

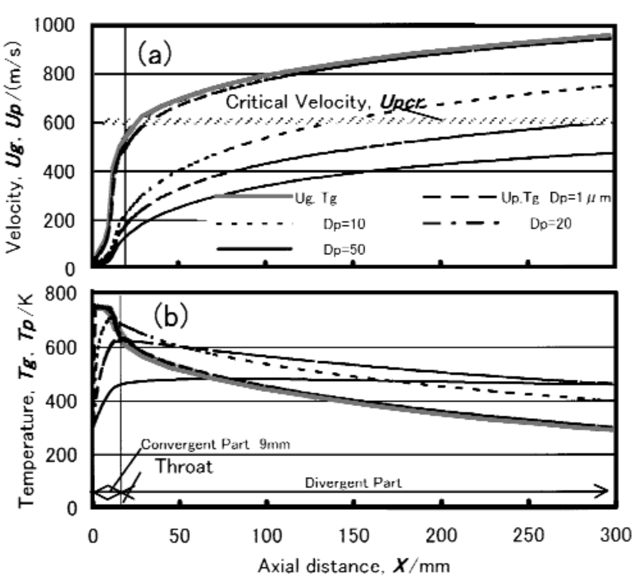

Fig. 8 Numerical simulation results with a change in particle diameter of Ni-Al-bronze powder by cold spray: (**a**) velocity of gas and particle and (**b**) temperature of gas and particle (baseline: $P_i = 2$ MPa, $U_{gi} = 0$ m/s, $T_{pi} = 750$ K, $U_{pi} = 10$ m/s, and $T_{pi} = 300$ K)

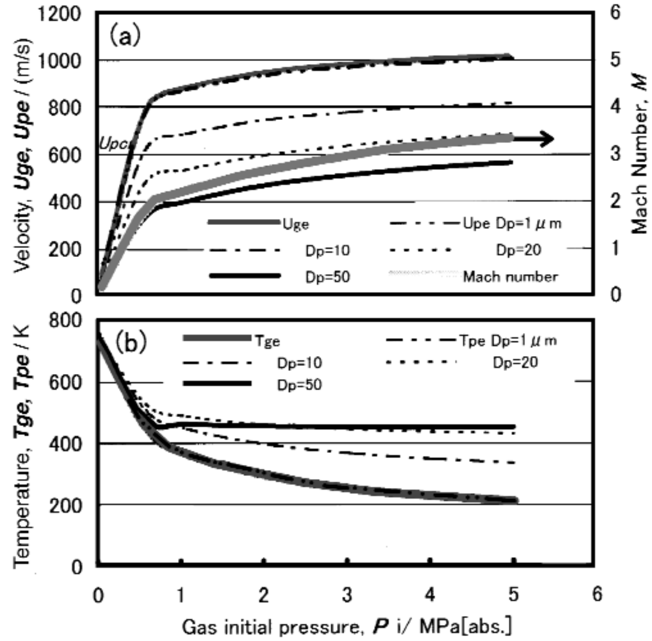

Fig. 9 Effect of gas initial pressure on the calculated results of cold spray process: (**a**) velocity of gas and Ni-Al bronze particle and (**b**) temperature of gas and particle ($U_{gi} = 0$ m/s, $T_{gi} = 750$ K, $U_{pi} = 10$ m/s, and $T_{pi} = 300$ K)

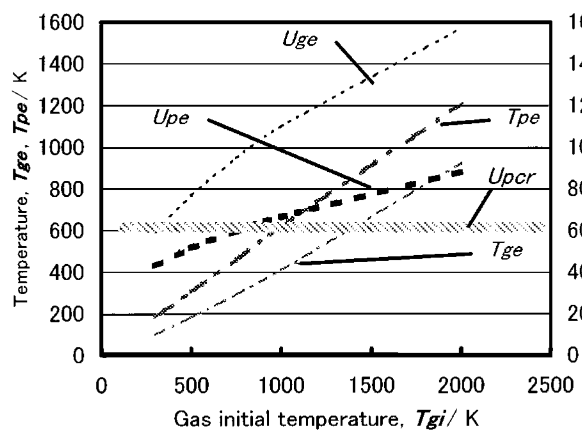

Fig. 10 Effect of gas initial temperature on the calculated results of cold spray process: velocity of gas and Ni-Al bronze particle (20 μm), temperature of gas and particle ($P_i = 2$ MPa, $U_{gi} = 0$m/s, $U_{pi} = 10$ m/s, and $T_{pi} = 300$ K)

the de Laval nozzle exit and gas temperature decreases to 290 K under the baseline initial conditions; gas pressure of 2.0 MPa [abs], temperature of 750 K, and velocity of 0 m/s and particle temperature of 300 K and velocity of 10 m/s. Ni-Al bronze particles 20 μm and smaller reach the critical velocity.

- The initial gas pressure and temperature affect accelerating particles in the cold spray process. The initial gas velocity has a slight influence.

Acknowledgments

The authors thank graduate student Tetsuya Minamida and students Hiroyuki Simomura, Naoki Huruhashi, and Hideaki

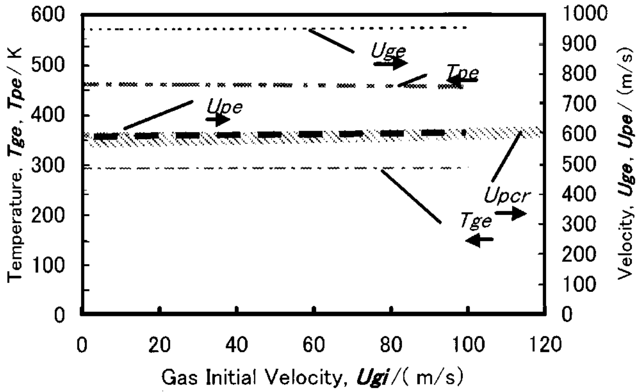

Fig. 11 Effect of gas initial velocity on the calculated results of cold spray process: velocity of gas and Ni-Al bronze particle (20 μm), temperature of gas and particle (P_i = 2 MPa, T_{gi} = 750 K, U_{pi} = 10 m/s, and T_{pi} = 300 K)

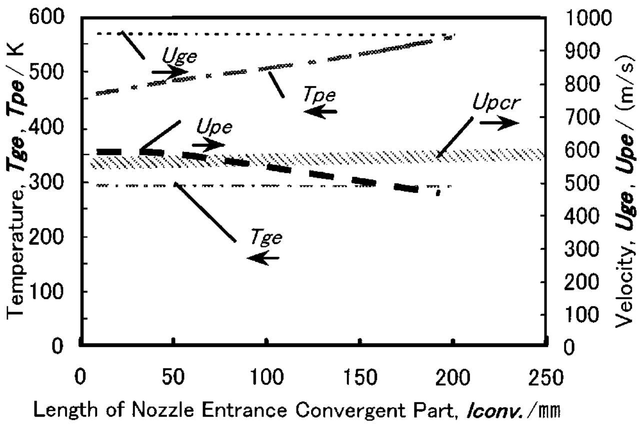

Fig. 12 Effect of length of nozzle entrance convergent part on the calculated results of cold spray process: velocity of gas and Ni-Al bronze particle (20 μm), temperature of gas and particle (baseline: P_i = 2 MPa, U_{gi} = 0 m/s, T_{pi} = 750 K, U_{pi} = 10 m/s, and T_{pi} = 300 K)

Saitou, Shinshu University, for their assistance. This study was supported by grants-in-aid for Scientific Research from the Ministry of Education, Science, Sports and Culture, Government of Japan. The project number is 11750620.

References

1. David L. Mason and Kris Rao: in *Thermal Spray Coatings—New Materials, Processes and Applications,* F.N. Longo, ed., American Society for Metals, Metals Park, OH, 1984, pp. 51-63.
2. K.A. Kowaisky, D.R. Marantz, M.F. Smith, and W.L. Oberkampf: in *Thermal Spray Research and Applications,* T.F. Bernecki, ed., ASM International, Materials Park, OH, 1990, pp. 587-92.
3. *Product Catalogue Diamond Jet,* Sulzer Metco (US) Inc., New York, NY, 1995.
4. *Product Catalogue Carbide Jet System (CJS),* OZU-Mashinenbau GmbH, Castrop-Rauxel, Germany, 1995.
5. M.L. Thope and H.J. Richer: in *Thermal Spray: International Advances in Coating Technology,* C.C. Bernt, ed., ASM International, Materials Park, OH, 1992, pp. 137-47.
6. G.R. Heath and R.J. Dumola: in *Thermal Spray: Meeting the Challenges of the 21st Century,* C. Coddet, ed., ASM International, Materials Park, OH, 1998, pp. 1495-1500.
7. C.M. Hackette and G.S. Settles: *Thermal Spray Science and Technology,* C.C. Berndt and S. Sampath, eds., ASM International, Materials Park, OH, 1995, pp. 135-40.
8. K. Sakaki, Y. Shimizu, Y. Gouda, and A. Devasenapathi: in *Thermal Spray: Meeting the Challenges of 21st Century,* C. Coddet, ed., ASM International, Materials Park, OH, 1998, pp. 445-50.
9. K. Kopiola, J.P. Hirvonen, L. Laas, and F. Rossi: J. *Thermal Spray Technol.,* 1997, vol. 6 (4), pp. 469-74.
10. K. Sakaki, Y. Shimizu, N. Saitoh, and Y. Gouda: *J. Jpn. Thermal Spraying Soc.,* 1997, vol. 34 (1), pp. 1-9 (in Japanese).
11. K. Sakaki, Y. Shimizu, Y. Gouda, and T. Minamida: *J. Jpn. Thermal Spraying Soc.,* 1998, vol. 35 (3), pp. 195-203 (in Japanese).
12. K. Sakaki, Y. Shimizu, and Y. Gouda: *J. Jpn. Inst. Met.,* 1999, vol. 63 (2), pp. 269-76 (in Japanese).
13. R.B. Bhhgat, M.F. Amateau, A. Papyrin, J.C. Conway, Jr., B. Stutaman, and B. Jones: in *Thermal Spray: A United Forum for Science and Technological Advances,* C.C. Berndt, ed., ASM International, Materials Park, OH, 1997, pp. 361-67.
14. P. Gougeon, C. Moreau, V. Lacasse, M. Lamontage, I. Powell, and A. Bewsher: *Adv. Processing Tech. Particulate Mater.,* 1994, vol. 6, pp. 199-210.
15. For example, K. Matuo: *Compressible Fluid Dynamics,* Rikougakusha, Tokyo, 1994, p. 83.
16. R. Clift, J.R. Grace, and M.E. Weber: *Bubbles, Drops and Particles,* Academic Press, New York, NY, 1987.
17. *JSME Heat Transfer Handbook,* Japan Society of Mechanical Engineers, Tokyo, 1993, p. 44 (in Japanese).
18. A.P. Alkhimov, V.F. Kosarev, and A.N. Papyrin: *Dokl. Akad. Nauk USSR,* 1990, vol. 315, pp. 1062-65 (in Russian).